Chapter 10

Induction Motors with Rotor Helical Motion

Ebrahim Amiri and Ernest Mendrela

Additional information is available at the end of the chapter

http://dx.doi.org/10.5772/48056

1. Introduction

A demand for sophisticated motion control is steadily increasing in several advanced application fields, such as robotics, tooling machines, pick-and-place systems, etc. These kinds of applications require implementation of at least two or more conventional motors/actuators, often operating with different type of mechanical gear. Electric motors/actuators that are able directly perform complex motion (with multiple degrees of mechanical freedom – multi-DoMF) may provide appreciable benefits in terms of performances, volume, weight and cost.

This chapter is organized as follows. Section 2 provides a brief overview of the main typologies of induction motors with two degrees of mechanical freedom (IM-2DoMF) structure. Section 3 introduces the mathematical model for helical-motion induction motors. Section 4 discusses the phenomenon known end effect caused by finite length of the armature and its negative influences on the motor performance. Section 5 presents a construction of a twin-armature rotary-linear induction motor with solid double layer rotor, its design data and the performance prediction of the motor. The results obtained from FEM modeling are then verified by the test carried out on experimental model of the motor what validates the theoretical modeling of the motor.

2. Topologies of induction motors with two degrees of mechanical freedom

Several topologies of electromagnetic motors featuring a multi-DoMF structure were investigated in the technical literatures (Mendrela et al., 2003, Krebs, et al., 2008). Considering the geometry, three classes of motors can be distinguished:

- X-Y motors – flat structure
- Rotary-linear motor – cylindrical geometry
- Spherical motors – spherical geometry

2.1. X-Y motors

X-Y motors, also called planar motors, are the machines which are able to translate on a plane, moving in the direction defined by two space co-ordinates. They may be usefully employed for precision positioning in various manufacturing systems such as drawing devices or drive at switch point of guided road/e.g. railway. The representative of X-Y motors is shown schematically in Fig. 1. Primary winding consist of two sets of three phase windings placed perpendicularly to one another. Therefore, magnetic traveling fields produced by each winding are moving perpendicularly to one another as well. Secondary part can be made of non-magnetic conducting sheet (aluminum, copper) backed by an iron plate. The motor with a rotor rectangular grid-cage winding is another version that can be considered.

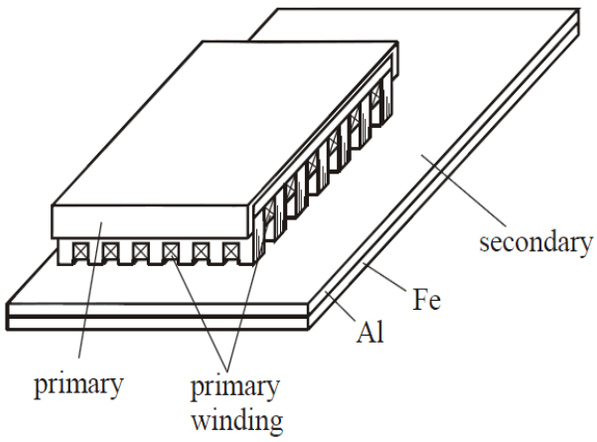

Figure 1. Construction scheme of X-Y induction motor (Mendrela et al., 2003).

The forces produced by each of traveling fields can be independently controlled contributing to the control of both magnitude and direction of the resultant force. This in turn controls the motion direction of the X-Y motor.

2.2. Rotary-linear motors

Mechanical devices with multiple degrees of freedom are widely utilized in industrial machinery such as boring machines, grinders, threading, screwing, mounting, etc. Among these machines those which evolve linear and rotary motion, independently or simultaneously, are of great interest. These motors, which are able effectively generate torque and axial force in a suitably controllable way, are capable of producing pure rotary motion, pure linear motion or helical motion and constitute one of the most interesting topologies of multi-degree-of freedom machines (Bolognesi et al., 2004). Some examples of such actuators have already been the subject of studies or patents (Mendrela et al., 2003, Giancarlo & Tellini, 2003, Anorad, 2001). A typical rotary-linear motor with twin-armature is shown in Fig. 2. A stator consists of two armatures; one generates a rotating magnetic field, another traveling magnetic field. A solid rotor, common for the two armatures is applied. The rotor consists of an iron cylinder covered with a thin copper layer. The rotor cage winding that looks like grid placed on cylindrical surface is another version that can be applied. The direction of the rotor motion depends on two

forces: linear (axially oriented) and rotary, which are the products of two magnetic fields and currents induced in the rotor. By controlling the supply voltages of two armatures independently, the motor can either rotate or move axially or can perform a helical motion.

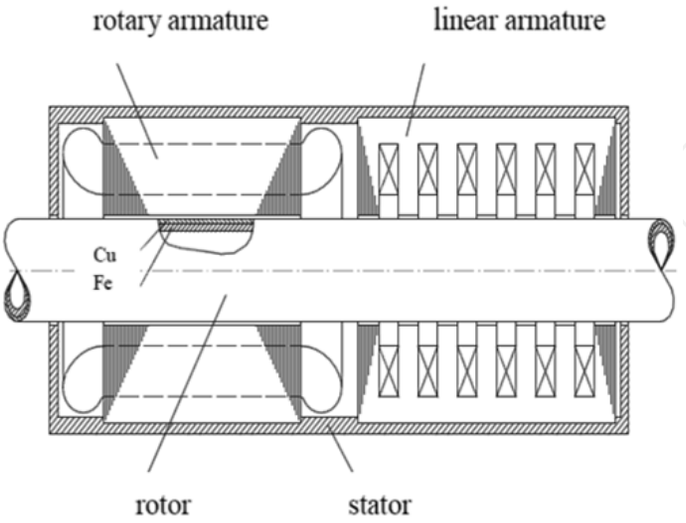

Figure 2. Scheme of twin armature rotary-linear induction motor (Mendrela et al., 2003).

2.3. Spherical motors

The last class of multi-DoMF motors has spherical structure. The rotor is able to turn around axis, which can change its position during the operation. Presently, such actuators are mainly proposed for pointing of micro-cameras and laser beams, in robotic, artificial vision, alignment and sensing applications (Bolognesi et al., 2004). In larger sizes, they may be also used as active wrist joints for robotic arms. Fig. 3 shows one of the designs in which the rotor driven by two magnetic fields generated by two armatures moving into two directions perpendicular to one another. This design is a counterpart of twin-armature rotary-linear motor.

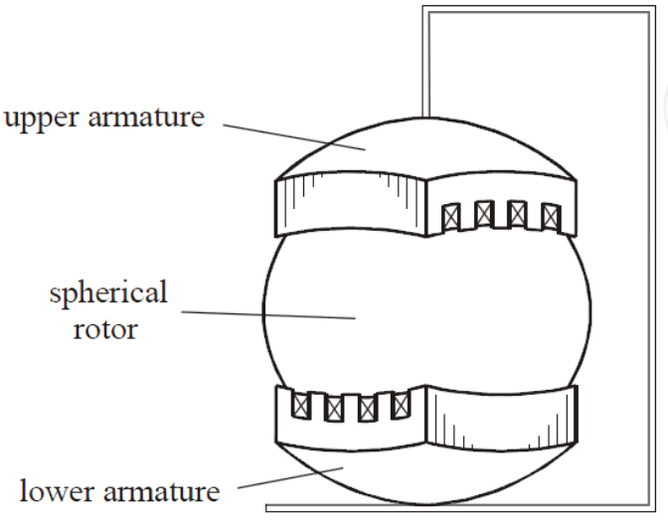

Figure 3. Construction scheme of twin-armature induction motor with spherical rotor (Mendrela et al., 2003).

3. Mathematical model of induction motor with magnetic field moving helically

The basic and most comprehensive research on IM-2DoMF is contained in the book (Mendrela et al., 2003). The analysis of these motors is based on theory of the induction motors whose magnetic field is moving in the direction determined by two space coordinates. According to this theory the magnetic field of any type of motor with 2DoMF can be represented by the sum of two or more rotating-traveling field what allows to consider the complex motion of the rotor as well as end effects caused by the finite length of stator. In the next subsections a sketch of theory of the motor with the rotating-traveling magnetic field whose rotor is moving with helical motion is presented.

3.1. Definition of magnetic field and rotor slip

3.1.1. Magnetic field description

The magnetic field moving helically in the air-gap is represented by the magnetic flux density B wave moving in the direction placed between two co-ordinates z and θ (Fig. 4).

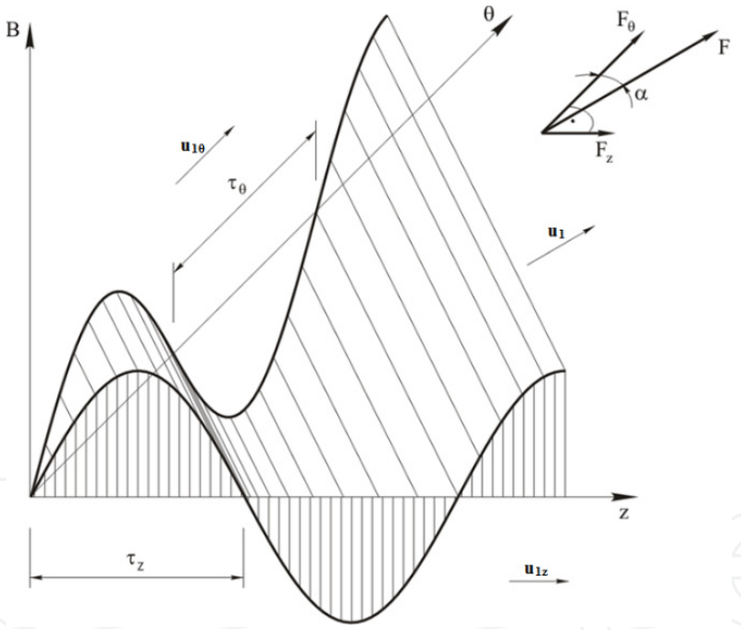

Figure 4. Magnetic field wave moving into direction between two spaces coordinates (Mendrela et al., 2003).

It can be expressed by the following formula (Mendrela et al., 2003):

$$B = B_m \exp\left[j\left(\omega t - \frac{\pi}{\tau_\theta}\theta - \frac{\pi}{\tau_z} z \right)\right] \tag{1}$$

where B_m - amplitude of travelling wave of magnetic flux density, ω - supply pulsation, τ_θ and τ_z - pole-pitch length along θ and z axes.

The physical model of the motor which could generate such a field is shown in Fig. 5.

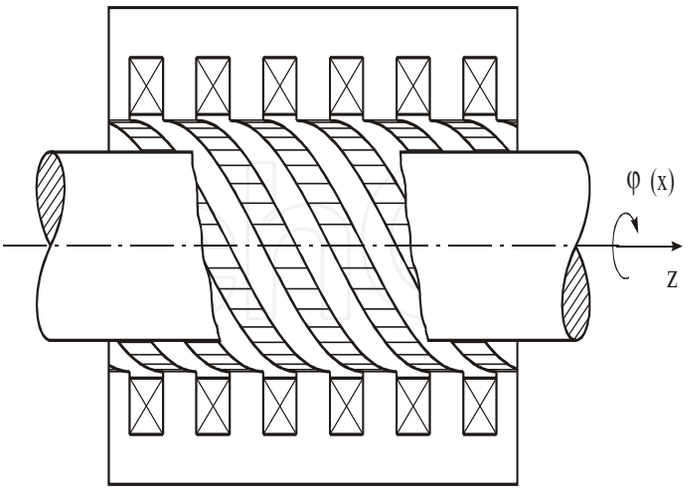

Figure 5. Rotary-linear induction motor with rotating-traveling magnetic field (Mendrela et al., 2003).

The electromagnetic force that exerts on the rotor is perpendicular to the wave front and can be divided into two components: F_z – linear force, F_θ - rotary component (Fig. 4). The relationships between force components are:

$$\frac{F_\theta}{F_z} = ctg\ \alpha\ , \qquad F_\theta = F\ cos\ \alpha \tag{2}$$

where,

$$ctg\alpha = \frac{\tau_z}{\tau_\theta} \tag{3}$$

3.1.2. Rotor slip

To derive a formula for the rotor slip the motor is first considered to operate at asynchronous speed. Meaning, an observer standing on the rotor surface feels a time variant magnetic field. Therefore, magnetic field for a given point $P(\theta_1 z_1)$ (Fig. 6) on the rotor surface is varying in time and expressed by the following equation:

$$B(t, \theta_1, z_1) = B_m \exp\left[j\left(\omega t - \frac{\pi}{\tau_\theta}\theta_1 - \frac{\pi}{\tau_z}z_1\right)\right] = var \tag{4}$$

Eqn. (4) is true if:

$$\omega t - \frac{\pi}{\tau_\theta}\theta_1(t) - \frac{\pi}{\tau_z}z_1(t) = \psi(t) \tag{5}$$

where $\psi(t)$ is the angle between point P and the wave front of the magnetic field wave. Differentiating Eqn. (5) with respect to time t yields:

$$\omega - \frac{\pi}{\tau_\theta}\omega_\theta - \frac{\pi}{\tau_z}u_z = \omega_2 \tag{6}$$

where ω_2 (slip speed) is the angular speed of point P with respect to the stator field and ω_θ and u_z are the angular and linear speeds of the rotor, respectively.

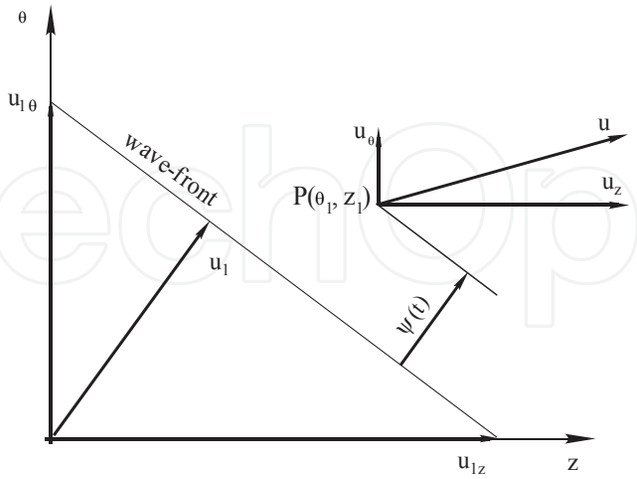

Figure 6. Rotary-linear slip derivation (Mendrela et al., 2003).

The, field velocities along θ and z axes are expressed by the equations:

$$\omega_{1\theta} = 2\tau_\theta f \quad , \qquad u_{1z} = 2\tau_z f \tag{7}$$

Inserting (7) to (6), it takes the form:

$$\omega - \frac{\omega}{\omega_{1\theta}}\omega_\theta - \frac{\omega}{u_{1z}}u_z = \omega_2 \tag{8}$$

Similarly, as in the theory of conventional induction motors, it can be written:

$$\omega_2 = \omega s \tag{9}$$

From (8) and (9) the following equation for the rotor slip is finally derived:

$$s_{\theta z} = 1 - \frac{\omega_\theta}{\omega_{1\theta}} - \frac{u_z}{u_{1z}} \tag{10}$$

The two dimensional rotor slip obtained in Eqn (10) is a function of rotary and linear rotor speed components as well as the speeds of the magnetic field moving along two space coordinates. If the motion of rotor is blocked along one of the coordinates, this slip takes the form known for motors with one degree of freedom. For example: if the rotor is blocked in the axial direction, the u_z component drops to zero and the slip takes the form:

$$s_\theta = 1 - \frac{\omega_\theta}{\omega_{1\theta}} \tag{11}$$

which is the form of rotor slip in the theory of conventional induction motor.

3.2. Motor equivalent circuit

For the induction motor with rotating-travelling field the equivalent circuit is shown in Fig. 7, which corresponds to the well-known circuit of rotary induction motor. The only

difference is in the rotor slip, which for rotary-linear motor depends on both rotary and linear rotor speeds.

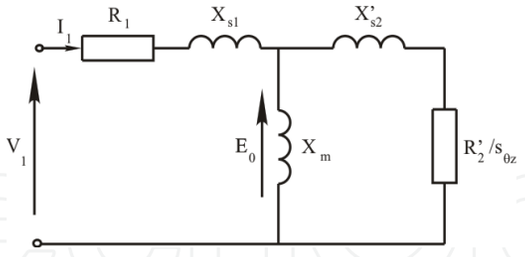

Figure 7. Equivalent circuit of induction motor with rotating-travelling magnetic field.

Similarly to the conventional rotary motors, the secondary resistance can be split into two resistances as shown in Fig. 8. R_2' represents the power loss in the rotor windings and the second part $(R_2' \frac{1-s_{\theta z}}{s_{\theta z}})$ contributes to mechanical power P_m.

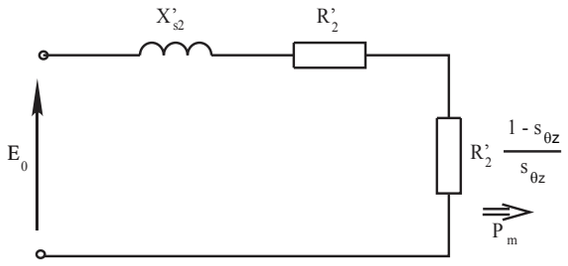

Figure 8. Equivalent circuit of rotor of rotary-linear induction motor.

The mechanical power of the resultant motion between θ and z axis is proportional to the resistance $R_2' \frac{1-s_{\theta z}}{s_{\theta z}}$ and is equal to:

$$P_m = mR_2' \frac{1-s_{\theta z}}{s_{\theta z}} I_2'^2 \tag{12}$$

where m is the number of phases.

Inserting Eqn (10) into Eqn (12), it takes the form:

$$P_m = mI_2'^2 \frac{R_2'}{s_{\theta z}} \left(\frac{\omega_\theta}{\omega_{1\theta}} + \frac{u_z}{u_{1z}}\right) \tag{13}$$

The resultant mechanical power P_m can be expressed in the form of its component in θ and z direction:

$$P_m = P_{m\theta} + P_{mz} \tag{14}$$

From (11), (13) and (14):

$$P_{m\theta} + P_{mz} = mR_2' \frac{1-s_\theta}{s_{\theta z}} I_2'^2 + mR_2' \frac{1-s_z}{s_{\theta z}} I_2'^2 \tag{15}$$

Therefore, Fig. 8 can be redrawn in terms of the resistance split into two components as shown in Fig. 9.

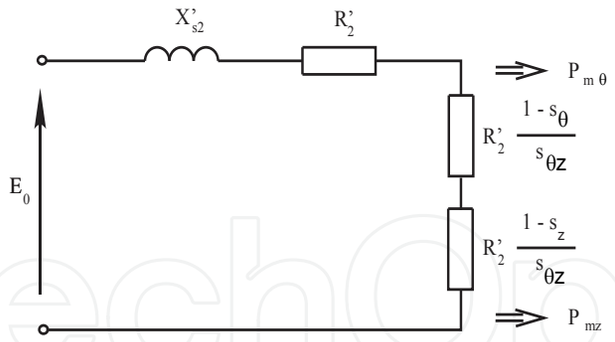

Figure 9. Equivalent circuit of rotor of rotary-linear induction motor with mechanical resistance split into two components.

3.3. Electromechanical characteristics

Unlike conventional rotary motors with the curvy characteristics of electromechanical quantities versus slip, electromechanical quantities in rotary-linear motor cannot be interpreted in one dimensional shape and should be plotted in a surface profile as a function of either slip $s_{\theta z}$ or speed components u_θ and u_z. The circumferential speed u_θ is expressed as follows:

$$u_\theta = R_r \,.\, \omega_\theta \tag{16}$$

where R_r is the rotor radius.

As an example, the force-slip characteristic of a typical rotary-linear motor is plotted in Fig. 10.

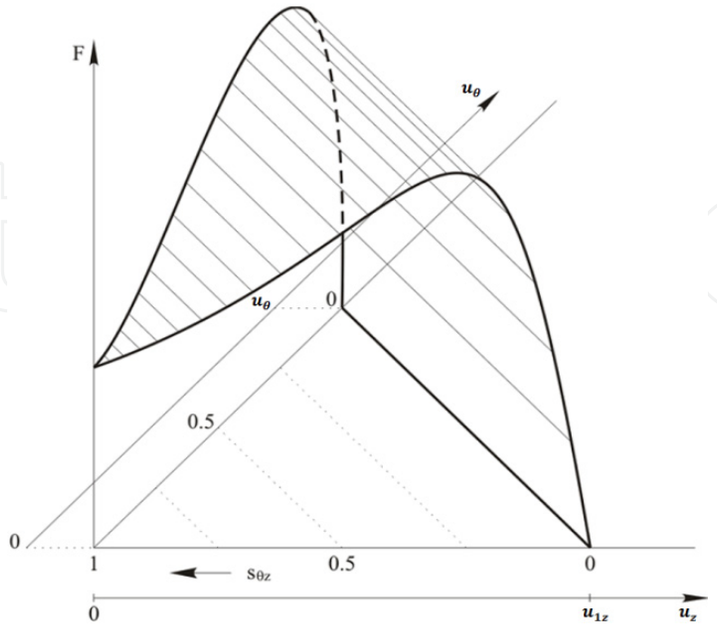

Figure 10. Fig. 10. Electromechanical characteristic of the induction motor with a rotating-travelling field (Mendrela et al., 2003).

In order to determine the operating point of the machine set, let the rotor be loaded by two machines acting independently on linear (axial) and rotational directions with the load force characteristics shown in Fig. 11.

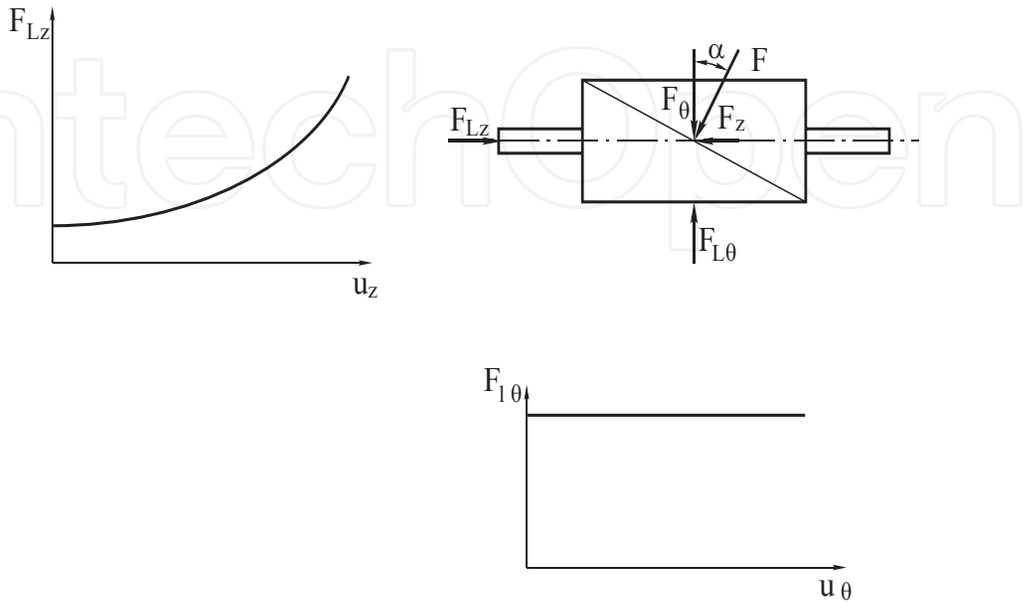

Figure 11. Load characteristics for IM-2DoMF, F_{lz}: load force in axial direction, $F_{l\theta}$: load force in rotary direction.

The equilibrium of the machine set takes place when the resultant load force is equal in its absolute value and opposite to the force developed by the motor. The direction of the electromagnetic force F of the motor is constant and does not depend on the load. Thus, at steady state operation both load forces $F_{l\theta}$ and F_{lz} acts against motor force components F_θ and F_z in the same direction if the following relation between them takes place:

$$\frac{F_\theta}{F_z} = \frac{F_{l\theta}}{F_{lz}} = ctg\alpha = \frac{\tau_z}{\tau_\theta} \tag{17}$$

To draw both load characteristics on a common graph, the real load forces $F_{l\theta}$ and F_{lz} acting separately on rotational and linear directions should be transformed into $F'_{l\theta}$ and F'_{lz}, forces acting on the direction of the motor force *F*. These equivalent forces are:

$$F'_{l\theta} = \frac{F_{l\theta}}{\cos\alpha} \quad , \quad F'_{lz} = \frac{F_{lz}}{\sin\alpha} \tag{18}$$

The transformed load characteristics drawn as a function of u_θ and u_z, as shown in Fig. 12, are the surfaces intersecting one another along the line segment $\overline{KA}$. This line segment that forms the $F_l(u)$ characteristic is a set of points where the following equation is fulfilled:

$$F'_{l\theta} = F'_{lz} \tag{19}$$

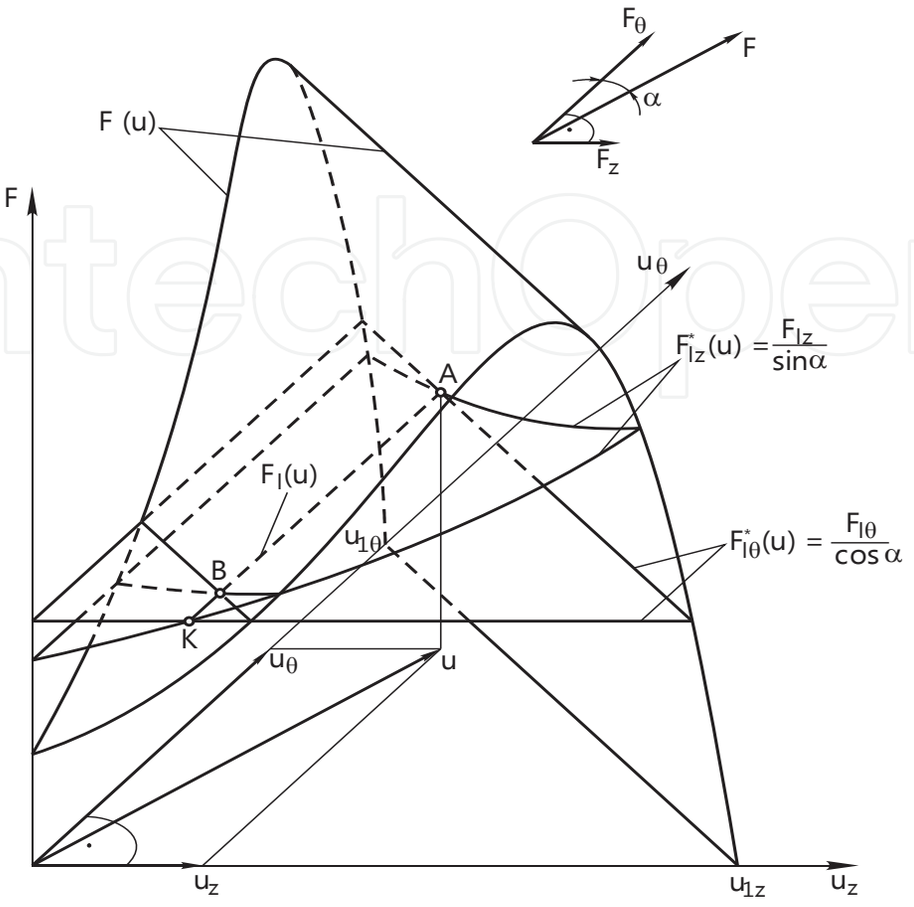

Figure 12. Determination of the operating point A of the machine set with IM-2DoMF (Mendrela et al., 2003).

The load characteristic $F_l(u)$ intersects with the motor characteristic at points A and B, where the equilibrium of the whole machine set takes place. To check if the two points are stable the steady state stability criterion can be used, which is applied to rotary motors in the following form:

$$\frac{dF}{du} < \frac{dF_l(u_\theta, u_z)}{du} \tag{20}$$

$$\frac{dF_{l\theta}}{du_\theta} > 0, \quad \frac{dF_{lz}}{du_z} > 0 \tag{21}$$

Applying this criterion, point A in Fig. 12 is stable and point B is unstable.

3.4. Conversion of mathematical model of IM-2DoMF into one of IM-1DoMF

The mathematical model of IM-2DoMF presented in previous subsections is more general than the one for linear or rotating machines. The rotating magnetic field wave of rotating

machines and the traveling field of linear motors are in the mathematical description special cases of the rotating–traveling field. If the wave length remains steady, pole pitches along both axis (τ_θ and τ_z) will vary by changing the motion direction of field waves. For example: if the wave front (see Fig. 4) turns to θ axis, then $\tau_z = \infty$. This makes the formula (1) changes to:

$$B = B_m \exp\left[j\left(\omega t - \frac{\pi}{\tau_\theta}\theta \right) \right] \tag{22}$$

which is the flux density function for rotary motor. The $\alpha = 0$ and according to Eqn (2) the force $F = F_\theta$ what is the case for rotary motors. On the other hand, turning the wave completely toward z axis leads to infinity pole pitch value along θ axis ($\tau_\theta = \infty$). By inserting this into Eqn (1) and (10) the description of both field and slip expressed by two space coordinates turns to the description of such quantities in linear motors.

In other word, the mathematical model of the rotary-linear motor is a general form of conventional, one dimensional motors and can be reduced at any time to the model either of rotary or linear motors.

4. Edge effects in rotary-linear induction motors

The twin-armature rotary-linear induction motor, which is the object of this chapter consists of two armatures what makes this machine a combination of two motors: rotary and tubular linear, whose rotor are coupled together. This implies that the phenomena that take place in each set of one-degree of mechanical freedom motors also occur in the twin armature rotary-linear motor in perhaps more complex form due to the complex motion of the rotor. One of these phenomena is called end effects and occurs due to finite length of the stator at rotor axial motion. This phenomenon is not present in conventional rotating induction machines, but play significant role in linear motors.

These effects are the object of study of many papers (Yamamura, 1972, Greppe et all, 2008, Faiz & Jafari, 2000, Turowski, 1982, Gierczak & Mendrela, 1985, Mosebach et all, 1977, Poloujadoff et all, 1980). In the literature, end effects are taken into account in various ways. In the circuit theory a particular parameter can be separated from the rest of equivalent circuit elements, and it represents the only phenomena that are caused by finite length of primary part of linear motor. This approach has been done in (Pai et all, 1988, Gieras et all, 1987, Hirasa et all, 1980, Duncan & Eng, 1983, Mirsalim et all, 2002). Kwon et al, solved a linear motor (LIM) with the help of the FEM, and they suggested a thrust correction coefficient to model the end effects (Kwon et all., 1999). Fujii and Harada in (Fujii & Harada, 2000) modeled a rotating magnet at the entering end of the LIM as a compensator and reported that this reduced end effect and thrust was the same as a LIM having no end effects. They used FEM in their calculations. Another application of FEM in analysing LIMs is reported by (Kim & Kwon, 2006). A d-q axis equivalent model for dynamic simulation purposes is obtained by using nonlinear transient finite element analysis and dynamic end effects are obtained.

The end effect has been also included in the analysis of rotary-linear motors in the literature (Mendrela et al., 2003, Krebs et all, 2008, Amiri et all, 2011). This inclusion was done by applying Fourier's harmonic method when solving the Maxwell's equations that describe motor mathematically (Mendrela et al., 2003). This approach was also applied to study the linear motor end effects (Mosebach et all, 1977, Poloujadoff et all, 1980).

The edge effects phenomena caused by finite length of both armatures can be classified into two categories as follows:

- End effects: which occurs in the tubular part of the motor.
- Transverse edge effects: which exists in the rotary part.

4.1. End effects

One obvious difference between LIM and conventional rotary machines is the fact that in LIM the magnetic traveling field occurs at one end and disappears at another. This generates the phenomena called end effects. End effects can be categorized into two smaller groups called: static end effects and dynamic end effects.

4.1.1. Static end effects

This is the phenomenon which refers to the generation of alternating magnetic field in addition to the magnetic traveling field component. The process of generation of alternating magnetic field at different instances is shown in Fig. 13.

Instant t_1 = 0: The 3-phase currents are of the values shown by phasor diagram in Fig. 13.b and 13.c with maximum in phase A. The current distribution in the primary winding relevant to these values is shown in Fig. 13.a and its first space harmonic is represented by curve J in Fig. 13.b. The distribution of magneto-motive force F_m in the air-gap corresponding to this linear current density has the cosine form with the maximum value at both edges of the primary part shown in Fig. 13.b. This mmf generates the magnetic flux which consists of two components: alternating flux Φ_a shown in Fig. 13.a and traveling flux component. The distribution of these two components B_a and B_t as well as the resultant flux density ($B_a + B_t$) are shown in Fig. 13.c.

Instant t_2 = ¼ T (where T is sine wave period): The 3-phase currents are of value shown by phasor diagram in Fig. 13.d with zero in phase A. These currents make the distribution of the first harmonic of mmf F_m as shown in Fig. 13.d. Since there is no mmf at primary edges, the alternating flux component Φ_a does not occur and the traveling flux B_t is the only available component.

Instant t_3 = ½ T: After a half period, the currents are of values shown by phasor diagram in Fig. 13.e with the maximum negative value in phase A. The relevant mmf distribution reveals its maximum negative value at primary edges which generates the magnetic flux Φ_a represented by its flux density B_a (see Fig. 13.e) which adds to the traveling flux component B_t.

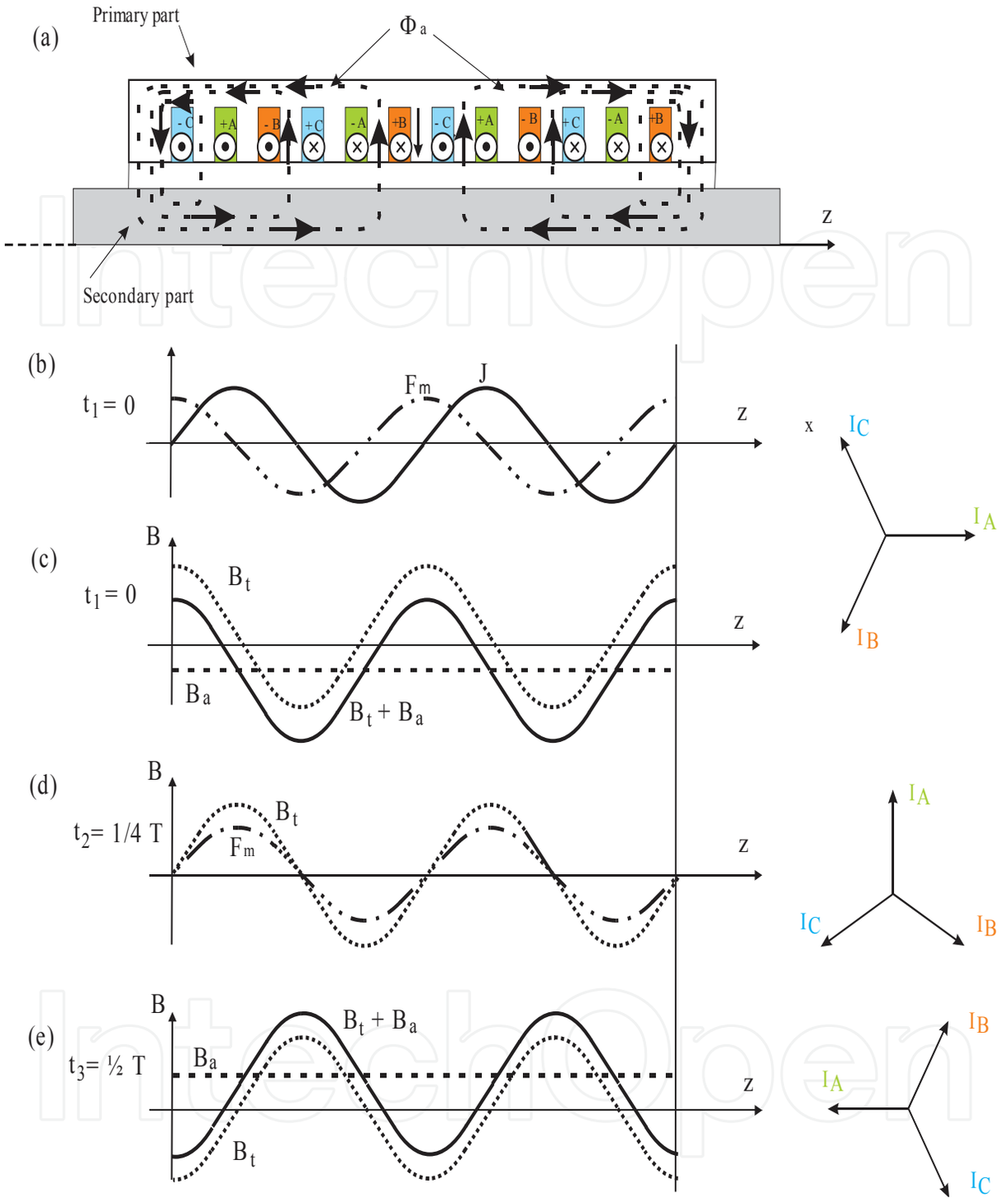

Figure 13. The process of generation of alternating magnetic field at different instances in 4-pole tubular motor: (Φ_a) – alternating component of magnetic flux, (B_a) – alternating component of magnetic flux density in the air-gap, (B_t) - travelling component of magnetic flux density in the air-gap, (J) – linear current density of the primary part, (F_m) – magneto-motive force of primary part in the air-gap.

Analysing the above phenomenon in time, one may find that magnetic flux density has two components: B_a which does not move in space but changes periodically in time called alternating component and B_t which changes in time and space is called traveling

component. The first component B_a does not exist in motors with infinity long primary part, which is the case in conventional rotary machines.

Summarizing, the resultant magnetic flux density distribution is a combination of the traveling wave component $B_t(t)$ and alternating magnetic field $B_a(t)$ denoted by:

$$B(t,z) = B_t \cos\left(\omega t - \frac{\pi}{\tau_p} z + \delta_m\right) + B_a \sin\left(\omega t - \frac{\pi}{\tau_p} + \delta_a\right) \tag{23}$$

where τ_p is pole pitch and δ_m is phase angle.

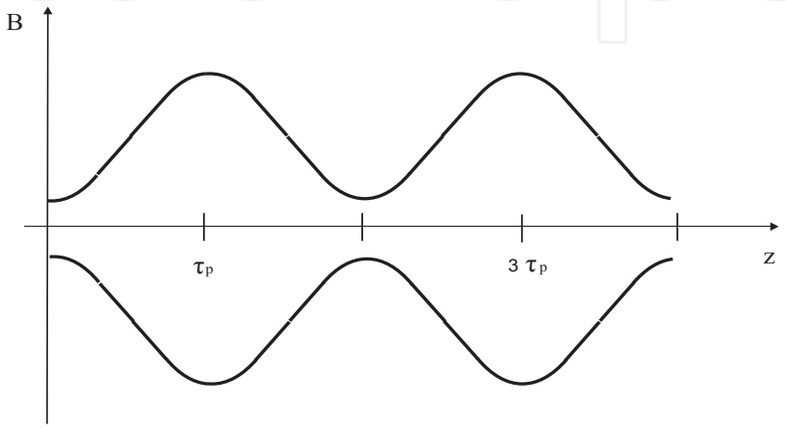

Figure 14. The envelope of the resultant magnetic flux density in the air-gap of four pole linear motor due to presence of the alternating magnetic field (τ_p - pole pitch).

When only the travelling wave exists, the envelop of flux density distribution in the air gap is uniform over the entire length of the primary core but the second term deforms the air gap field distribution to the shape shown in Fig. 14. The alternating flux contributes to the rising of additional power losses in the secondary and to producing of braking force when one part of LIM motor is moving with respect to the other one (Mosebach et all, 1977, Poloujadoff, et all, 1980, Amiri, et all, 2011). This component occurs no matter what is the value of the speed of the secondary part (Poloujadoff, 1980). The envelope of the resultant magnetic flux density for the four-pole motor is no longer uniform as shown in Fig. 14.

4.1.2. Dynamic end effects

The dynamic end effects are the entry and exit effects that occur when the secondary moves with respect to the primary part. This phenomenon will be explained in two stages:

Stage I: secondary part moves with synchronous speed

There are no currents induced in the rotor (within the primary part range) due to traveling magnetic field component (since the secondary moves synchronously with travelling field). However, the observer standing on the secondary (see Fig. 15) feels relatively high change of magnetic flux when enters the primary part region and when leaves this region at exit edge. This change contributes to rising of the eddy currents at both the entry and exit edges. These

currents damp the magnetic field in the air-gap at entry in order to keep zero flux linkage for the secondary circuit. At the exit edge the secondary eddy currents tries to sustain the magnetic flux linkage outside the primary zone the same as it was before the exit. This leads to damping magnetic flux at the entry edge and to appearance of magnetic flux tail beyond the exit edge (Fig. 16.a). The distribution of the primary current J_1 is uniform over the entire region. The envelop of the eddy currents induced in the secondary J_2 shown in Fig. 16.a is relevant to the magnetic flux density distribution in the air-gap.

The eddy currents at the entry and exit edges attenuate due to the fact that the magnetic energy linked with these currents dissipate in the secondary resistance. Thus, the lower is the secondary resistance the more intensive is damping at entry and the longer is the tail beyond the exit.

Stage II: rotor (secondary part) moves with a speed less than the synchronous speed

The currents are induced in the secondary over the entire primary length due to slip of the secondary with respect to the travelling component of primary magnetic flux. These currents superimpose the currents that are due to the entry and exit edges. The resultant eddy current envelop is shown schematically in Fig. 16.b. The flux density distribution in the air-gap and current density in the primary windings are also shown in Fig. 16.b. As it is illustrated the primary current density is uniformly distributed along the primary length only if the coils of each phase are connected in series and the symmetry of 3-phase currents is not affected by the end effects. The magnetic flux density distribution has the same shape and changes in a same pattern in both stages, but due to the rotor current reaction, the second stage has a lower magnetic flux density (B). However, primary current density is higher at the second stage if the primary winding is supplied in these two cases with the same voltage.

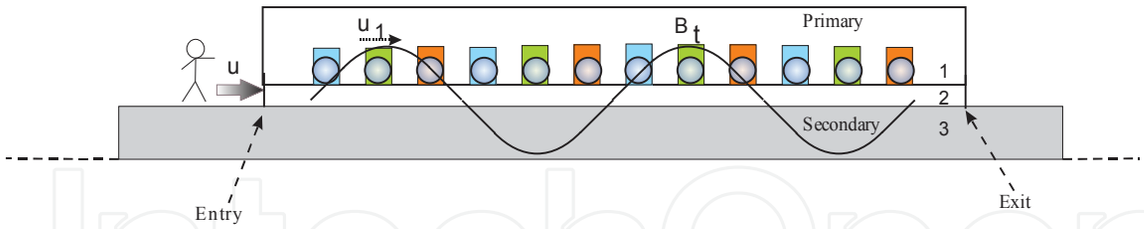

Figure 15. End effect explanation: (B_t) - travelling component of magnetic flux density in the air-gap (u_1) speed of traveling magnetic field (u) speed of the rotor.

In general, end effect phenomena leads to non-uniform distribution of:

- magnetic field in the air-gap,
- current in the secondary,
- driving force density,
- power loss density in the secondary.

Thus, this contributes to:

- lower driving force,
- higher power losses,

- lower motor efficiency,
- lower power factor.

Due to dynamic end effects, the resultant magnetic flux density in the air-gap can be expressed as a summation of three flux density components as follows (Greppe, et all, 2008):

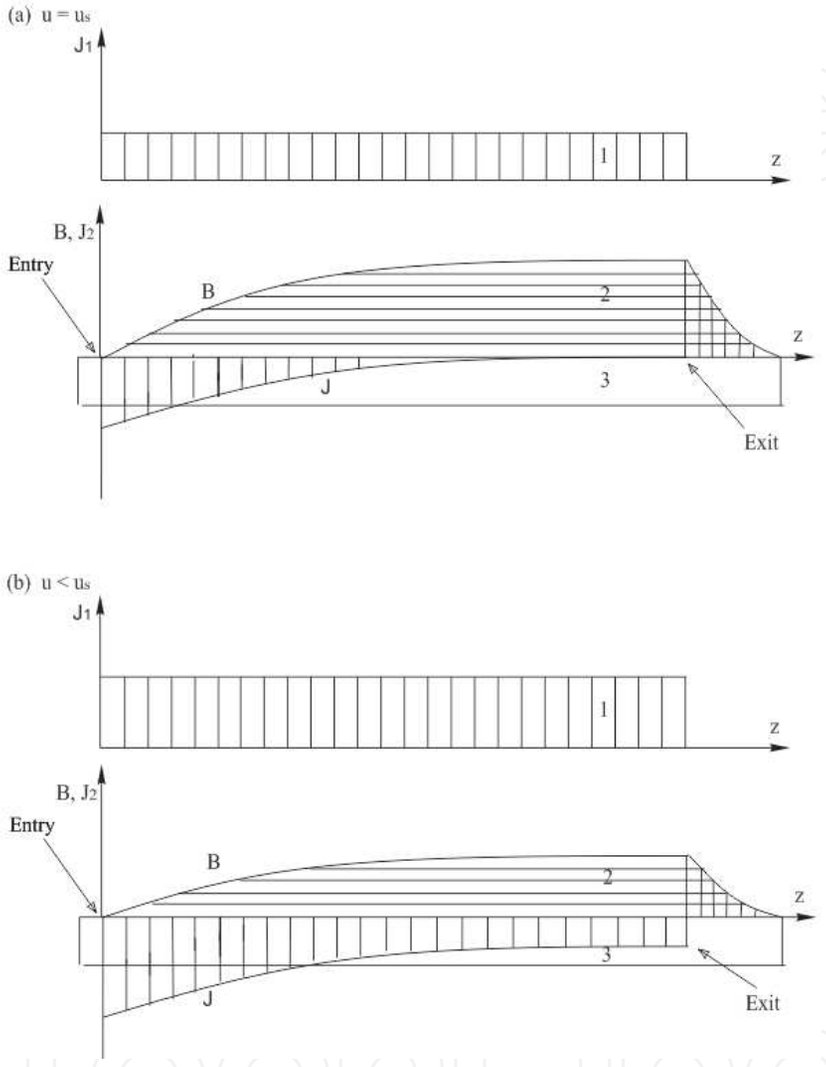

Figure 16. Distribution of primary current (J_1), secondary current (J_2) and magnetic flux density in the air-gap (B): (a) u =u_1 (b) u < u_s.

$$B(t,z) = B_t \cos\left(\omega t - \frac{\pi}{\tau_p} z + \delta_m\right) + B_1 e^{-z/\alpha_1} \cos\left(\omega t - \frac{\pi}{\tau_{pe}} z + \delta_1\right) + B_2 e^{+z/\alpha_2} \cos\left(\omega t + \frac{\pi}{\tau_{pe}} z + \delta_2\right) \quad (24)$$

All the three terms of this equation have the same frequency and are steady with respect to time t. The first term is the traveling wave moving forward at synchronous speed. The second term is an attenuating traveling wave generated at the entry end, which travels in the positive direction of z and whose attenuation constant is $1/\alpha_1$ and its half-wave length is τ_{pe}. The third term of Eqn (24) is an attenuating traveling wave generated at the exit end, which travels in the negative direction and whose attenuation constant is $1/\alpha_2$ and

half-wave length is τ_{pe}. The B_1 wave is caused by the core discontinuity at the entry end and the B_2 wave is caused by the core discontinuity at the exit end, hence, both are called end effect waves. Both waves have an angular frequency ω, which is the same as that of power supply. They have the same half wave-length, which is different from half-wave length (equal to pole pitch) of the primary winding. The traveling speed of the end waves is given by $v_e = 2\,f\,\tau_{pe}$ and is the same as the secondary speed if high speed motors is studied. However, in low speed motors, the speed of the end waves can be much higher than that of secondary (Yamamura, 1972). The length of penetration of entry end wave α_1 depends on motor parameters such as gap length and secondary surface resistivity. The impact of these parameters on α_1 are quiet different at high speed motors and low speed motors. As a result, α_1 is much longer at high speed motors with respect to low speed motors. Also, in the high-speed motors, half wave length τ_{pe} is almost linearly proportional to the speed of secondary and is independent from gap length and secondary surface resistivity while it is dependent to such parameters at low speed motors (Yamamura, 1972). Therefore, the speed of the end waves is equal to the secondary speed at high speed motors regardless the value of parameters such as supply frequency, gap length and surface resistivity, while in low speed motors, end wave's speed depends on such parameters and may reach to even higher than synchronous speed at low slip region. The super-synchronous speed of the end-effect wave at motor speed lower and close to synchronous speed occurs only in low speed motors (Yamamura, 1972).

The entry-end-effect wave decays relatively slower than the exit-end-effect wave and unlike exit-end-effect wave, is present along the entire longitudinal length of the air-gap and degrades the performance of the high speed motor. The exit-end-effect wave attenuates much faster due to the lack of primary core beyond the exit edge. Therefore, the influence of the exit field component B_2 on motor performance is less than that of the entry component B_1, and it may be disregarded for many applications Gieras et all, 1987, Hirasa et all, 1980, Greppe, et all, 2008).

For the motors with the number of magnetic pole pairs greater than 2 if the synchronous speed is below 10 m/s the end effects can be ignored. For the motors with higher synchronous speeds the influence of end effects can be seen even for the motors with higher number of pole-pairs (Mendrela, 2004).

4.2. Transverse edge effects

The transverse edge effect is generally described as the effect of finite width of the flat linear motor and is the result of x component of eddy current flowing in the solid plate secondary (Fig. 17.b). Since, there are no designated paths for the currents, as it is in cage rotors of rotary motors, the currents within the primary area are flowing in a circular mode (Fig. 17.b). These currents generate their own magnetic field, whose distribution is shown schematically in Fig. 17.a. This magnetic field shown schematically as B_r in Fig. 18 subtracts from the magnetic field B_s generated by the primary part winding. The resultant field has non-uniform distribution in transverse direction (x axis) (Fig. 19). This

non-uniform distribution of the magnetic field and circular pattern of the secondary currents contribute to the increase of power losses, decrease of motor efficiency and reduction of maximum electromagnetic force (Boldea & Nasar, 2001).

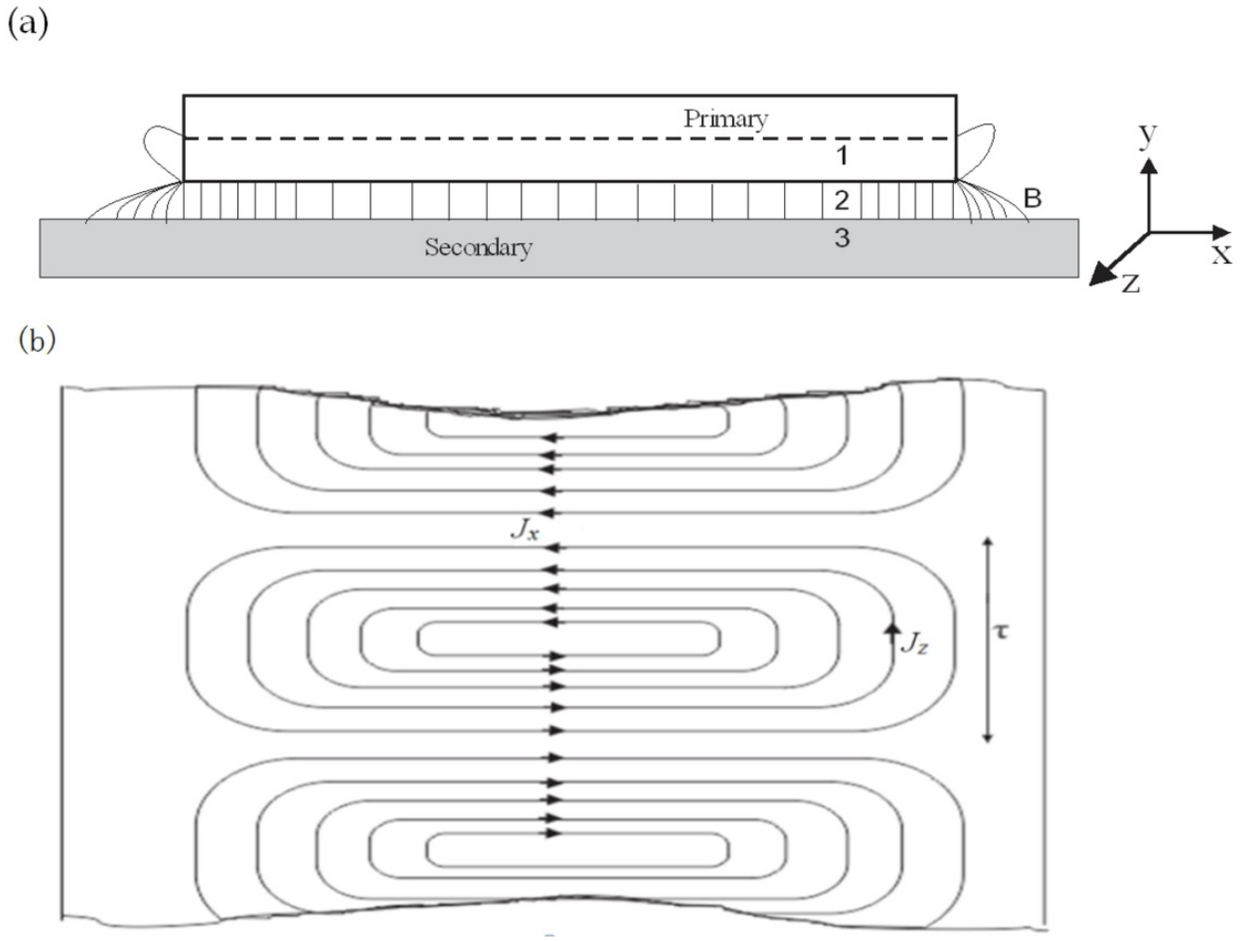

Figure 17. Transverse edge effect explanation: (a) The resultant magnetic flux distribution, (b) eddy current induced in the secondary.

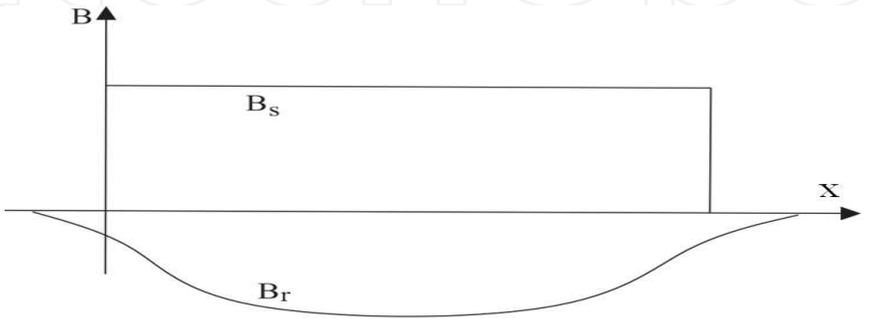

Figure 18. The distribution of magnetic flux density B_s produced by the primary current and B_r by the secondary currents.

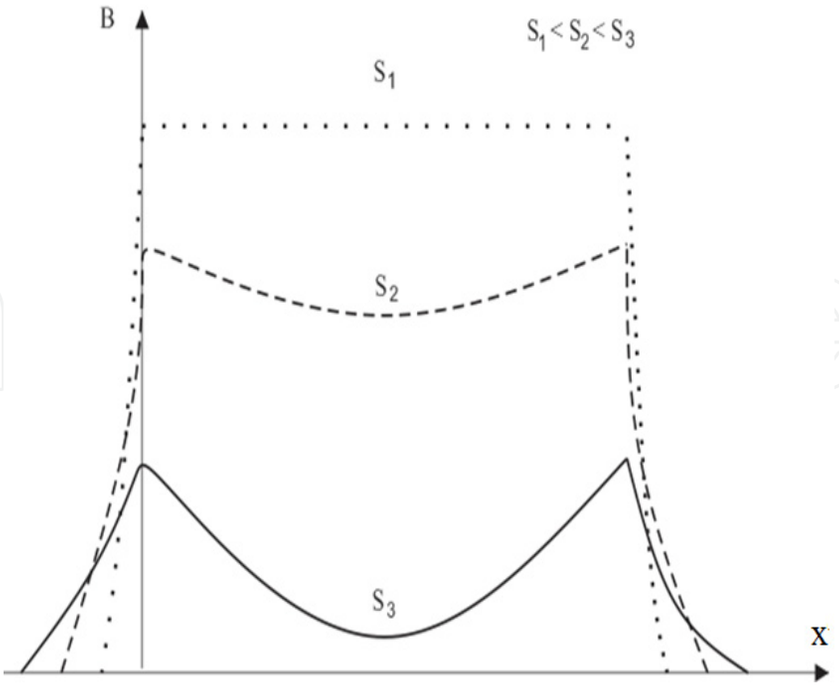

Figure 19. The resultant magnetic flux density distribution in the air-gap at different secondary slips.

As the rotary-linear motor is concerned, the transverse edge effect occurs for rotary armature. This effect has here more complex form due to the additional axial motion of the rotor. The above transverse edge effects superimpose on entry and exit effects whose nature is the same as discussed earlier for linear part of the rotary-linear motor. This motion makes the flux density distribution distorted as shown in Fig. 20. At the entry edge the flux density in the air-gap is damped, but at the exit edge it increases.

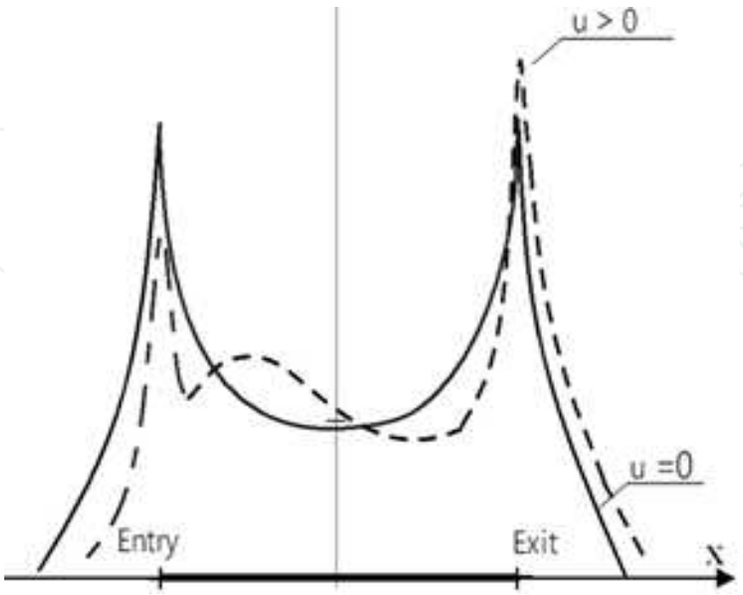

Figure 20. Resultant magnetic flux density in the air-gap of rotary part of the IM-2DoMF motor with linear speed greater than zero (u > 0).

5. Performance of twin-armature rotary-linear induction motor

5.1. Design parameter of the motor

One of a few design versions of rotary-linear motors is a Twin-Armature Rotary-Linear Induction Motor (TARLIM) shown schematically in Fig. 21. The stator consists of a rotary and linear armature placed aside one another. One generates a rotating magnetic field, another traveling magnetic field. A common rotor for these two armatures is applied. It consists of a solid iron cylinder covered with a thin copper layer. The direction of the rotor motion depends on two forces; linear and rotary, which are the products of two magnetic fields and currents induced in the rotor.

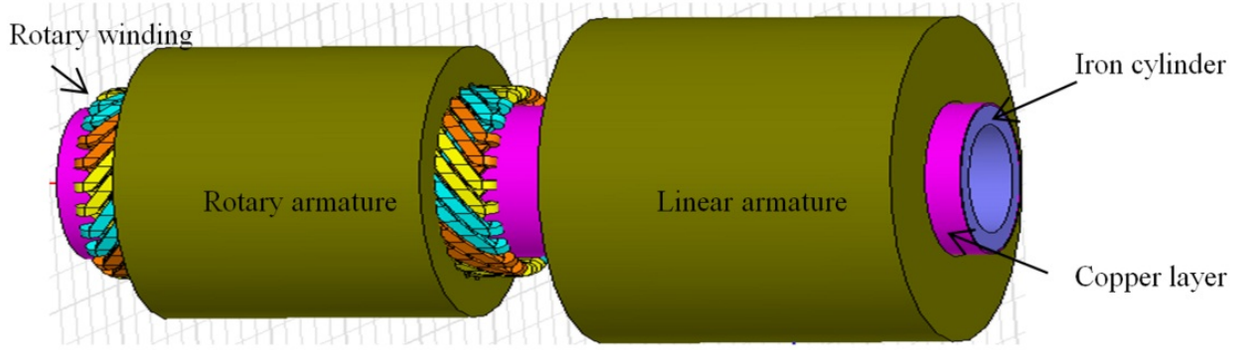

Figure 21. Schematic 3D-view of twin-armature rotary-linear induction motor.

The TARLIM in its operation can be regarded as a set two independent motors: a conventional rotary and tubular linear motor with the rotors joined stiffly. This approach can be applied only if there is no magnetic link between the two armatures, what practically is fulfilled due to the relatively long distance between the armatures and the low axial speed of the rotors. In case of the motor analysed here both conditions are satisfied and the analysis of each part of the TARLIM can be carried out separately as the analysis of IM 3-phase rotary and linear motors. The only influence of one motor on the other is during the linear motion of the rotor which will be considered at the end of this chapter.

To study the performance of TARLIM the exemplary motor has been chosen with the dimensions shown in Fig. 22. The dimensions of rotary armature are presented in details in Fig. 23.

The core of both armatures is made of laminated steel. The common rotor is made of solid steel cylinder covered by copper layer. Both armatures possess a 3-phase winding. The rotary and linear winding diagrams are shown in Figs. 24.a and 24.b, respectively. The winding parameters and the data of stator and rotor core material are enclosed in Table 1.

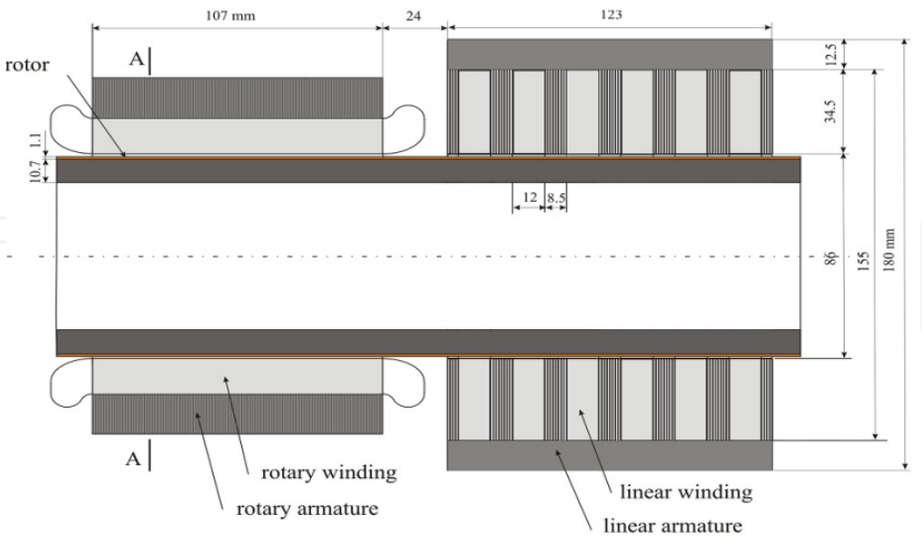

Figure 22. Dimensions of TARLIM chosen for analyse.

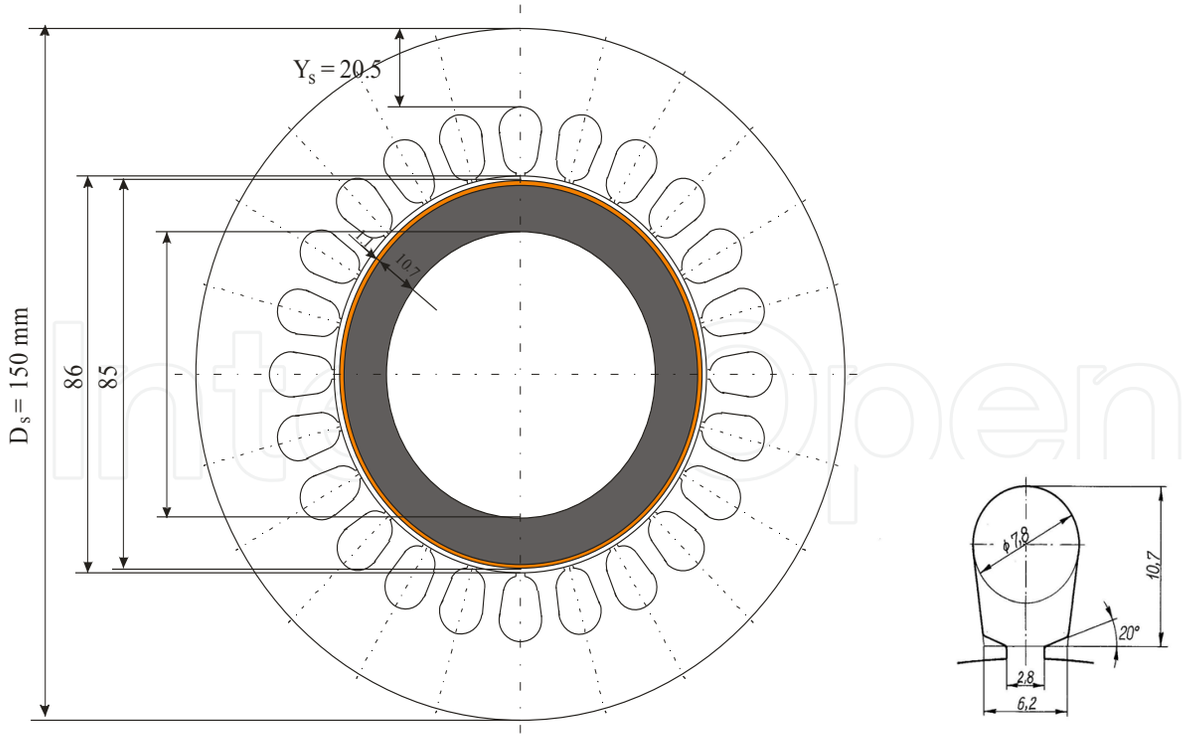

Figure 23. Rotary armature dimensions.

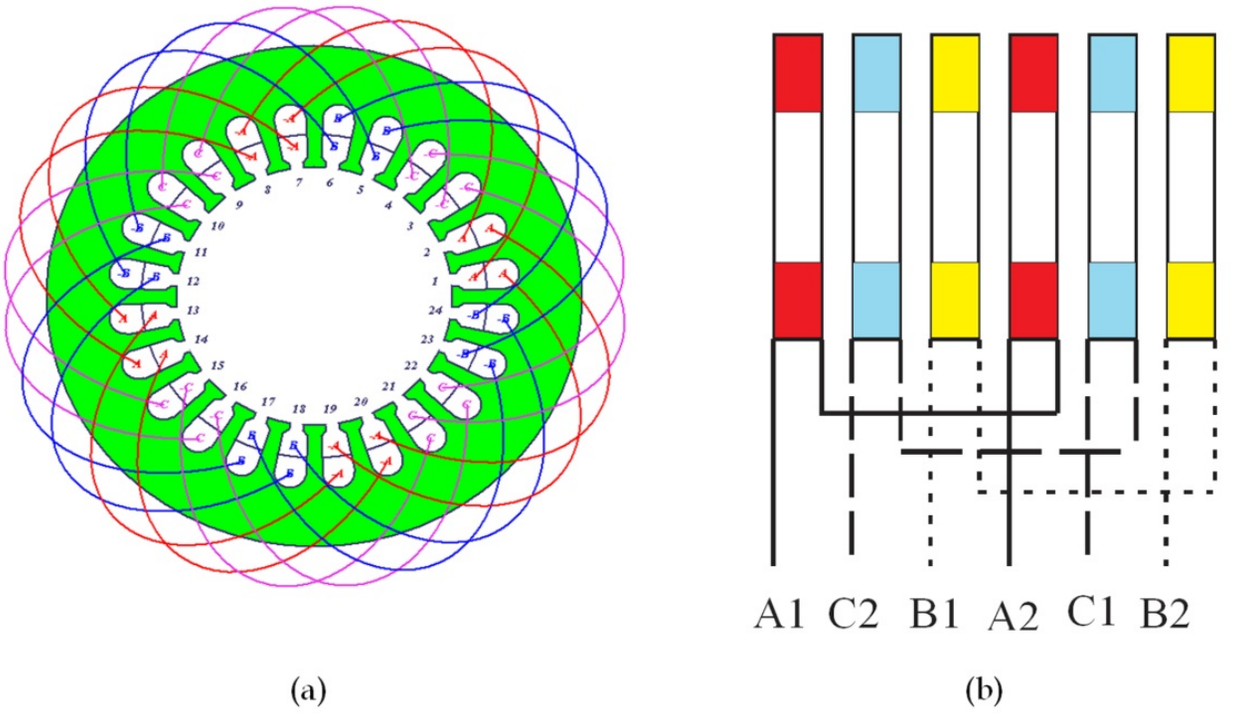

Figure 24. Winding diagram of the TARLIM, (a) rotary winding, (b) linear winding.

Linear winding data:	
Number of phases	3
Number of poles	2
Number of slots per pole per phase	1
Number of wires per slot, N_w	215
Copper wire diameter	1.29 mm
Rotary winding data:	
Number of phases	3
Number of poles	4
Number of slots per pole per phase	2
Number of wires per slot, Nw	96
Copper wire diameter	0.7 mm
Armature Core	Laminated steel
Air gap length, mm	0.5
Rotor	
Copper layer	
Thickness mm	1.1 mm
Conductivity ($\gamma_{Cu,@20C}$)	57.00x106 S/m
Solid iron cylinder	
Thickness mm	10.7 mm
Conductivity ($\gamma_{Fe,@20C}$)	5.91x106 S/m

Table 1. Winding and materials data for TARLIM.

5.2. Experimental model

To verify the modeling results, a real prototype of the motor was built (see Figs. 25 and 26) and tested. The laboratory model of TARLIM has a relatively short secondary length. Therefore, measuring motor performances at linear speed greater than zero was practically difficult so the test was carried out only at zero linear speed. The TARLIM operates practically at low rotary slip and at linear slip close to one. Thus the dynamic end effects does not influence much the motor performance but the static end effect caused by finite length of each of the armatures has a large impact on the linear motor performance.

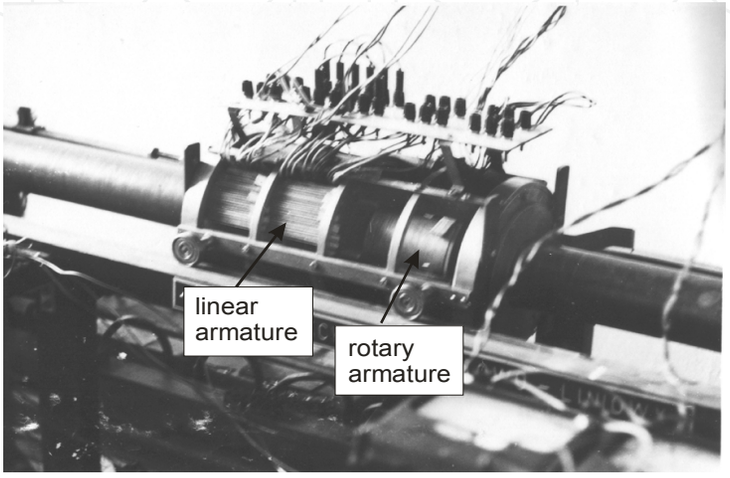

Figure 25. Laboratory model of twin-armature rotary-linear induction motor.

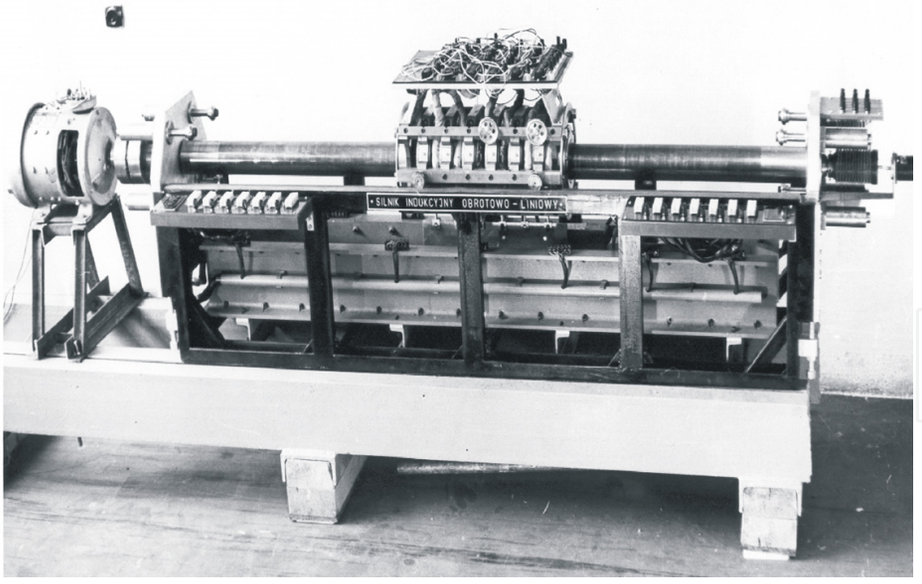

Figure 26. Measurement stand for testing of rotary-linear motors.

5.3. Motor performance

The analysis of each part of TARLIM performance is carried out separately as an independent tubular linear and rotary motor by 3-D FEM modelling.

The linear armature is being supplied from the constant voltage source of 86.6 V (rms), 50 Hz frequency. The results of simulation are shown in Figs. 27, 28 and 29 in form of the electromechanical force (F_{em}), mechanical power (P_m) and efficiency, respectively, versus linear slip of the rotor. These characteristics illustrate a significant impact of end effects on motor performance and are drawn as dashed line curves for the infinitely long motor when no end effects are considered, circles for the actual motor of finite armature length, when both static and dynamic end effects are taken into account and triangular sign for the experimental result.

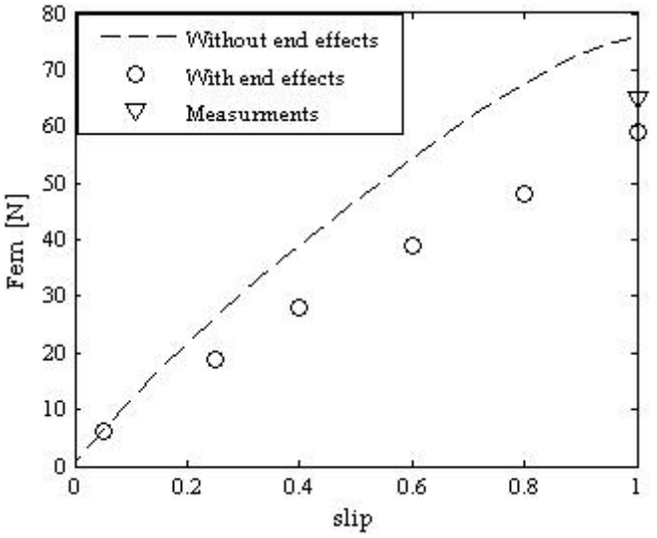

Figure 27. Characteristic of force vs linear slip.

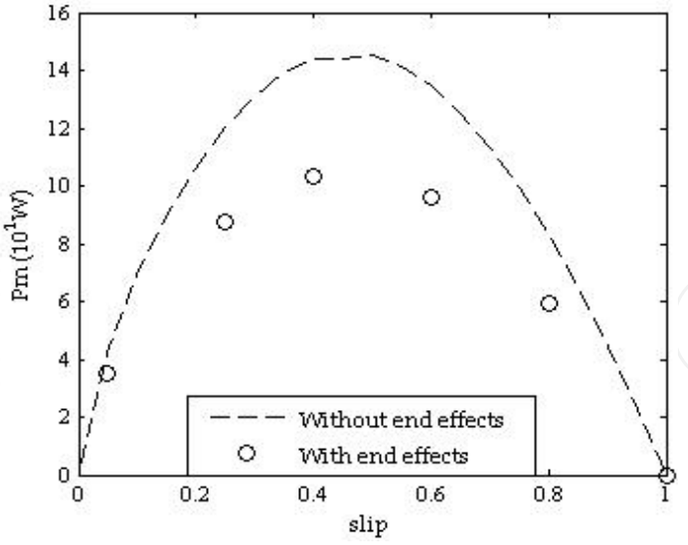

Figure 28. Characteristic of output power vs linear slip.

The motor under study has a linear synchronous speed equal to 6.15 m/s and is considered as low-speed motor. In low-speed motors, the speed of the end effect wave can be higher than the motor speed and even much higher than the synchronous speed, while in high-speed motors the speed of the end effect wave is about the same as the motor speed and

cannot be higher the synchronous speed. In low-speed motors, the attenuation of the entry end-effect wave is quick, while in high-speed motors the attenuation is very slow and the entry-end-effect wave presents over the entire longitudinal length of the air-gap. As a consequence of the difference, the influence of the end-effect wave on motor performance is also quite different at high-speed motors and low-speed motors. In low-speed motors, the end effect wave may improve motor performance in low-slip region, the important motor-run region, increasing thrust, power factor and efficiency, and allowing net thrust to be generated even at synchronous and higher speeds. On the contrary, in high speed motors, thrust, power factor and efficiency are reduced to a large extent in the low-slip region, and it is not an over statement to say that high-speed applications of linear induction motors may not be feasible if the end effect is overlooked and is allowed to remain as an influence.

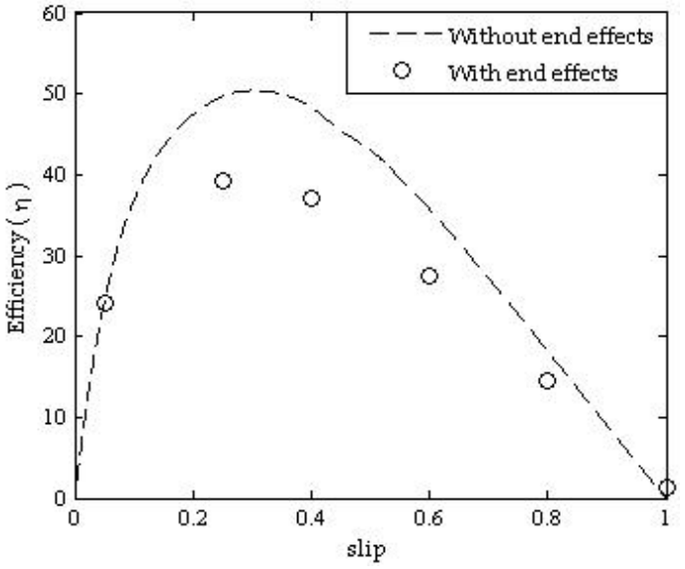

Figure 29. Characteristic of efficiency vs linear slip.

To study the performance of the motor at higher speeds, let us change the supply frequency to 3 times higher (synchronous speed, v_s= 3 * 6.15 m/s) and then recalculate the forces acted on rotor when all end effects are taken into account. Table 2 compares the output forces of the low-speed and high-speed motor at relatively low operational slip region.

Synchronous speed	Operational slip region	
	S=0.25	S=0.05
v_s= 6.15 m/s	19 N	6 N
v_s= 3*6.15 m/s	6 N	0 N

Table 2. Electromechanical force of low speed and high speed LIM.

The simulation of rotary part of the motor is done for the winding being supplied by the three-phase voltage of 150 V (rms), 50 Hz frequency.

Due to closed magnetic circuit in rotary armature, static end effect does not exist in rotational direction. However, the performance of rotary armature might be affected by dynamic end

effects during rotor axial motion. This is the only influence of linear part of TARLIM on rotary motion and, as stated earlier, both armatures have no more influence on one another due to the relatively long distance and the lack of magnetic interaction in between. To determine the influence of rotor axial motion on the performance of rotary armature, the characteristics of electromagnetic torque (T_{em}) and mechanical power (P_m) versus rotary slip at three different linear speeds (u = 0 m/s, u =3 m/s and u =6 m/s) along with experimental results at zero linear speed (u = 0 m/s) are plotted in Figs. 30 and 31. These effects contribute to diminishing of torque and all other rotary motor performances. One can observe that, the higher axial speed leads to lower rotary torque and mechanical power.

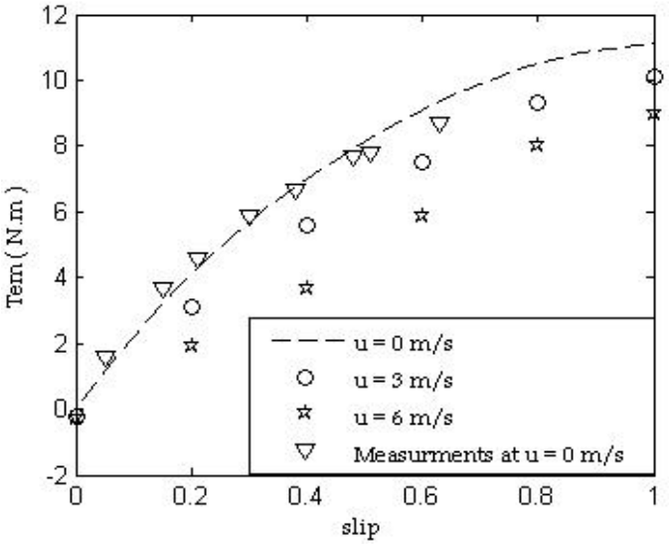

Figure 30. Characteristic of Torque vs rotary slip with and without linear motion.

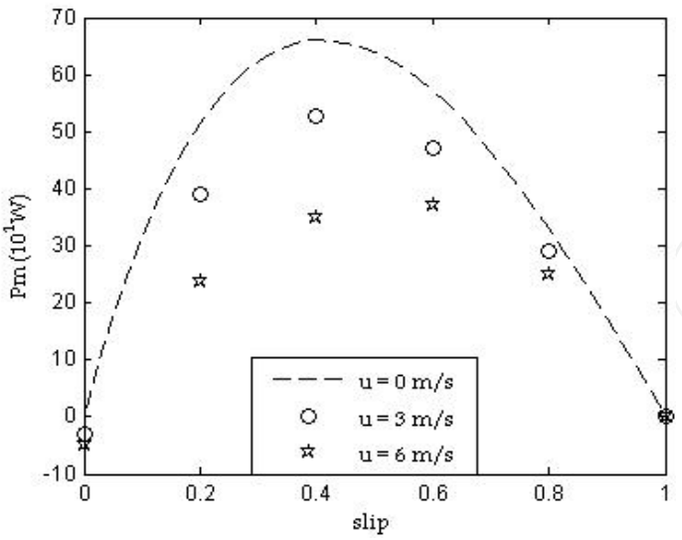

Figure 31. Characteristic of output power vs linear slip with and without linear motion.

Note, that the output quantities are extremely dependent on the property of materials. The conductivity of the materials used in 3D FEM analysis is kept constant, but in reality it might be influenced by the temperature. Therefore, minimal mismatch between

experimental measurements, where the temperature changes during the experiment and FEM results is expected. On the other hand, FEM needs as dense mesh as possible to compute quantities accurately, but the execution time of such a complicated model is enormous. Therefore, some trade-off between accuracy and execution time is required to obtain a good solution at reasonable cost. However, the discrepancies between test and simulation results are relatively small which validates the simulation models.

6. Conclusion

Rotary-linear induction motor is one of a few types of motors with two degrees of mechanical freedom. It may find application in robotics and special types of drives like machine tools and drilling machines. One of its representatives, the TARLIM, with two solid layer rotor was modelled in 3-D FEMM and its performance has been determined. The operation of the motor does not differ from the operation of machine set consisting rotary and tubular linear motor of which rotors are firmly coupled. The electromechanical performances of the motor are affected by the end effects which are familiar phenomena in linear machines. Practically, the impact of these phenomena is not significant in low axial speed of the rotor, what is expected for these types of motors.

The results obtained from the test carried out on the experimental model do not differ much from the ones got from simulations. Thus they validate the theoretical modeling of the motor.

Motor with the rotor cage made in form of grid placed on the cylindrical core is another version of TARLIM and is expected to have a better performance with respect to the solid two layer rotor.

Author details

Ebrahim Amiri and Ernest Mendrela
Louisiana State University, USA

7. References

Mendrela, E, Fleszar, J, Gierczak, E. (2003). *Modeling of Induction Motors With One and Two Degrees of Mechanical Freedom*, Norwell, MA: Kluwer Academic Publishers.

Krebs, G, Tounzi, A, Pauwels, B and Willemot, D. (2008). *General overview of integrated linear rotary actuators, in Proc. ICEM Conf.*

Bolognesi P, Bruno O, Landi A, Sani L, Taponecco L. (2004). *Electromagnetic actuators featuring multiple degrees of freedom:* a survey. In: ICEM conference, Krakow (Poland), 5–8 September.

Giancarlo, B and Tellini, B. (2003). *Helicoidal electromagnetic field for coilgun armature stabilization, IEEE Trans. Magn.*, vol. 39, no. 1, pp. 108–111, Jan. 2003.

Anorad Corp., New York, USA. (2001). *Rotary linear actuator*, U.S. Patent 6 215 206.

Yamamura, S. (1972). *Theory of Linear Induction Motors*, John Wiley & Sons.

Creppe, R. C, Ulson, J. A. C, Rodrigues, J. F. (2008). *Influence of Design Parameters on Linear Induction Motor End Effects*, *IEEE* Trans. Energy Convers., vol. 23, no. 2, pp. 358–362 June. 2008.

Faiz, J Jafari, H. (2000) *Accurate Modelling of Single-Sided Linear Induction Motor Considers End Effect and Equivalent Thickness,* IEEE Transactions on Magnetics, vol. 36, No. 5, September 2000, pp. 3785-3790.

Turowski, J. (1982). *Electromagnetic calculations of machine elements and electro mechanics*. WNT Warsaw, (in Polish).

Gierczak, E, Mendrela, E. (1985). *Magnetic flux, current, force and power loss distribution in twin-armature rotary-linear induction motor*, Scientia Electrica, Vo. 31, pp. 65-74, 1985.

Mosebach, H, Huhns, T, Pierson, E.S, Herman, D. (1977). *Finite Length Effects in Linear Induction Machines with Different Iron Contours*, IEEE Trans. On PAS-96, 1977, pp. 1087-1093.

Poloujadoff, M, Morel, B, Bolopion, A (1980). *Simultaneous Consideration of Finite Length and Finite Width of Linear Induction Motors,* IEEE Trans. On PAS, Vol. PAS-99, No. 3, 1980, pp. 1172-1179.

Pai, R.M., Boldea, I., and Nasar, S.A. (1988). *A complete equivalent circuit of a linear induction motor with sheet secondary*, IEEE. Trans., 1988, MAG-24, (1), pp. 639–654.

Gieras, J. F. , Dawson, G. E. and Eastham, A. R. (1987). *A new longitudinal end effect factor for linear induction motors, IEEE Trans. Energy Convers.*, vol. 2, no. 1, pp. 152–159, Mar. 1987.

Hirasa, T, Ishikawa, S and Yamamuro, T. (1980). *Equivalent circuit of linear induction motors with end effect taken into account*, *Trans. IEE Jpn.*, vol. 100, no. 2, pp. 65–71, 1980.

Duncan, J., and Eng, C. (1983) *Linear induction motor-equivalent circuit model'*, IEE Proc., Electr. Power Appl., 1983, 130, (1), pp. 51–57.

Mirsalim, M, Doroudi, A and Moghani, J. S. (2002). *Obtaining the operating characteristics of linear induction motors: A new approach*, IEEE Trans. Magn., vol. 38, no. 2, pp. 1365–1370, Mar. 2002.

Kwon, B. I, Woo, K. I. and Kim, S (1999). *Finite element analysis of direct thrust controlled linear induction motor*, IEEE Trans. Magn., vol. 35, no. 3, pp. 1306–1309, May 1999.

Fujii, N and Harada, T. (2000). *Basic consideration of end effect compensator of linear induction motor for transit*, in Industry Applications Conf., Oct. 8–12, 2000, pp. 1–6.

Kim, D.-k. and Kwon, B.-I. (2006). *A novel equivalent circuit model of linear induction motor based on finite element analysis and and its coupling with external circuits*, IEEE Trans. Magn., vol. 42, no. 10, pp. 3407–3409, Oct. 2006.

Krebs, G, Tounzi, A, Pauwels, B, Willemot, D and Piriou, F. (2008). *Modeling of a linear and rotary permanent magnet actuator*, IEEE Trans. Magn., vol. 44, no. 10, pp. 4357-4360, Nov. 2008.

Amiri, E, Gottipati, P, Mendrela, E. (2011). *3-D Space Modeling of Rotary-Linear Induction Motor With Twin-Armature* The 1st IEEE International Conference on Electrical Energy Systems, Chennai, Tamil Nadu, India, Jan 2011.

Poloujadoff, M. (1980). *The Theory of Linear Induction Machinery*, Oxford University Press, 1980.

Mendrela, E. (2004) *Electric Machines", Course Pack "Advanced Electric Machine*, Louisiana State University.

Boldea, I, Nasar, S.A.. (2001). *Linear Motion Electromagnetic Devices*, Taylor and Francis, 2001.